Green Chemistry

Reductive catalytic fractionation of agricultural residue and energy crop lignin and application of lignin oil as antimicrobials

Journal:	*Green Chemistry*
Manuscript ID	GC-ART-08-2020-002781.R1
Article Type:	Paper
Date Submitted by the Author:	20-Sep-2020
Complete List of Authors:	Ebikade, Osamudiamhen; University of Delaware, Chemical and Biomolecular Engineering; University of Delaware, Catalysis Center for Energy Innovation Samulewicz, Nicholas; University of Delaware, Chemical and Biomolecular Engineering Xuan, Shuangqing; University of Delaware, Animal and Food Sciences Sheehan, James; University of Delaware, Catalysis Center for Energy Innovation Wu, Changqing; University of Delaware, Animal and Food Sciences Vlachos, Dion; University of Delaware, Chemical and Biomolecular Engineering; University of Delaware, Catalysis Center for Energy Innovation

Reductive catalytic fractionation of agricultural residue and energy crop lignin and application of lignin oil as antimicrobials

Elvis Ebikade[1, 2], Nicholas Samulewicz[1, 2], Shuangqing Xuan[3], James D. Sheehan[1], Changqing Wu[3], and Dionisios G. Vlachos[1, 2]*

[1]*Catalysis Center for Energy Innovation, University of Delaware, 221 Academy Street, Newark, DE, 19716 USA.*
[2]*Department of Chemical and Biomolecular Engineering, University of Delaware, 150 Academy Street, Newark, DE, 19716 USA.*
[3]*Department of Animal and Food Sciences, University of Delaware, 531 S College Ave, Newark, DE, 19716 USA*
**Corresponding author: vlachos@udel.edu*

Abstract

Cheap and abundant waste from bioethanol and agricultural processing industries are an alluring alternative feedstock for biorefineries. In this work, we employ reductive catalytic fractionation (RCF) to depolymerize, over Ru/C powder and Ru/Al_2O_3 pellets, five herbaceous biomass feedstocks, namely corn stover, miscanthus, switchgrass, sugarcane bagasse, and wheat straw into phenolic monomers with high yields (~40 wt.% based on total (Klason + acid soluble) lignin and > 50 wt.% when stabilized using aldehydes), leaving behind a carbohydrate pulp residue. Interestingly, a polar solvent is sufficient to solubilize and fragment the lignin polymer into monomers without any catalyst. Contrary to woody biomass, where the monomer yields are positively correlated with the S-content of lignin, principal component analysis indicates that the monomer yields from herbaceous biomass depend on the content of lignin crosslinker – ferulate. Using NMR, we further identify α – 6 C-C linked oligomers formed from condensation reactions, explaining the unexpected low monomer yields of high β-O-4 herbaceous biomass. Recyclability experiments indicate that catalyst deactivation occurs through sintering, leaching, and fouling. Lignin oil from herbaceous biomass exhibits bacteriostatic effects against *Staphylococcus aureus*,

highlighting a potential application in functional food development and as food or feed preservative.

Keywords: Lignin, Valorization, Biomass, Antimicrobial Activity, Machine Learning, Biorefinery

Introduction

Globally, 1.5 billion tons per year of herbaceous or grassy biomass are produced inexpensively[1] in major grain growing regions. The US produces over 15.5 billion gallons of ethanol[2] annually, sourced mainly from corn, wheat straw and sugarcane. However, only the cellulosic portion of the biomass feedstock is currently utilized[3], having ramifications on the economics[4]. To combat this, valorizing the lignin-rich residue after sugar extraction for producing valuable aromatic compounds[5], rather than using it for low value applications, e.g., for heat and power[6], is appealing. Furthermore, estimated herbaceous biomass supply is 5 times that of woody biomass[7]. Yet, valorizing lignin from herbaceous agricultural residue has not received a commensurate level of attention in comparison to woody biomass, *e.g.*, hardwood and softwood. Prior reductive catalytic fractionation (RCF) studies have extensively focused on 'virgin' woody biomass[8,9] from poplar, pine, and birch wood, with little exploration of low-value agricultural residues or cheap energy crops. Herbaceous feedstocks are structurally distinct from woody biomass as they contain ester and ether-linked hydroxycinnamic acids, particularly, p-coumaric acid and ferulic acid, between lignin and xylans (Figure 1). These hydroxycinnamic acids have wide applications[10,11] as dietary supplements, food [12,13] and cosmetics additives[14].

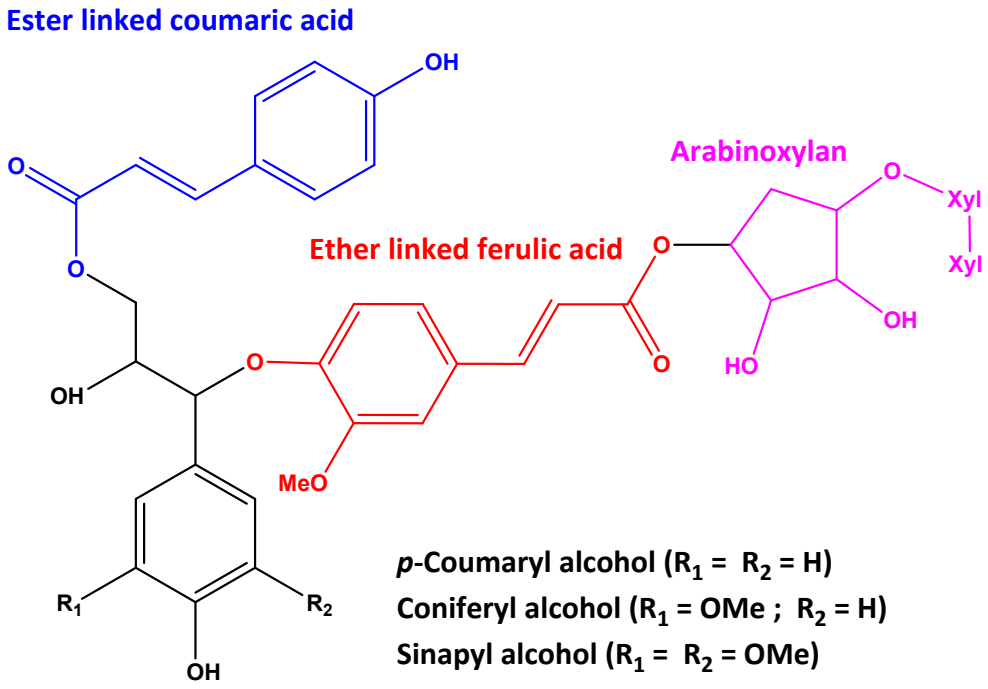

Figure 1. Lignin–carbohydrate complex in herbaceous feedstocks.

The coumarate units (Figure 1) are connected as pendant species to syringyl and guaiacyl monolignols in the lignin framework through ester bonds. The ferulate cross-links typical lignin monomers with xylans through ether or ester bonds (Figure 1)[1] and acts as a nucleation site for lignification in herbaceous feedstock[15].

Prior studies on herbaceous lignin depolymerization have mainly focused on corn stover[16–18] and miscanthus[19,20]. The simultaneous variation of hydrogenolysis conditions (*e.g.*, catalyst, temperature, solvent, time) in published studies[16,17,19,20] makes comparison among feedstocks difficult. Even though monomer yields from woody biomass correlate well with the S-content[20]/β-O-4[21,22] content, no reports correlate the product distribution with the lignin structure during hydrogenolysis of herbaceous crops. Herbaceous feedstocks have the highest β-O-4 content (>90%)[23–28] compared to 50 -70% in hard wood[23,25,26,29] and 30 – 40% in softwood[21]; yet, the monomer yields are much lower (30 – 40 wt.%[16,17,19,20]) than the theoretical maximum (~80 wt.% lignin monomer yields based on the β-O-4 content)[30]. This implies that the β-O-4 content is not a

good descriptor of monomer yields from herbaceous feedstocks, and some other component of the feedstock might serve as a better descriptor.

Direct hydrogenolysis of native biomass[20,31–34] over a heterogeneous metal catalyst is an effective method for cleaving the C-O bonds in lignin and producing aromatic monomers in high yields. However, there are no mechanistic studies describing the process by which lignin monomers are obtained from actual herbaceous feedstocks. Understanding the role of the solvent, catalyst, and process conditions on the RCF of these feedstocks is crucial towards gaining a fundamental understanding for optimizing performance. Also, ash in feedstocks can deactivate the catalyst[35,36], resulting in reduced monomer yields over multiple catalyst uses. Woody biomass has little (< 1 wt.% to negligible)[26,37,38] ash content, whose influence on RCF is slight and rarely studied. Conversely, herbaceous biomass has a much higher ash content (5-10 wt.% based on total biomass weight)[26] and thus, elucidating the impact of inorganics, which could leach from the feedstock, on RCF is necessary. Inorganics can be catalysts themselves[39,40] or can foul and electronically modify the catalyst active sites[36]. Therefore, evaluating the deactivation and recyclability of heterogeneous catalysts in herbaceous biomass processing is necessary.

In the present work, we evaluate five herbaceous agricultural residues and energy crops (corn stover, switchgrass, wheat straw, sugarcane bagasse, and miscanthus) for obtaining aromatic monomers through RCF. We perform mechanistic depolymerization studies with miscanthus to obtain insights into herbaceous feedstock conversion into phenolic monomers. We further compare the RCF of each feedstock under similar reaction conditions and explore the effect of biomass ash on catalyst recyclability. Characterization of the feedstocks, solubilized lignin monomers, oligomers and the residual carbohydrate pulp provides insights into the depolymerization of herbaceous biomass. Simple machine learning (principal component analysis) elucidates structure-

product distribution relationships, and the effect of ash on the catalyst recyclability is evaluated. With increased demand for biobased antimicrobials[41] for food[42] and cosmetic applications[14,43], we demonstrate the antimicrobial capabilities of the derived lignin oil from agricultural waste and energy crops, rather than model compounds or lignin-mimics as a sustainable solution.

Experimental Section

Chemicals and materials. All biomass samples were obtained from the Idaho National Laboratory[26] and fully characterized using the NREL LAP protocols[44]. The syringol (S), guaiacol (G), and hydroxyphenol (H) content was determined using the thioacidolysis method described by Harman Ware *et al.*[45], detailed in the SI. The samples were milled to particles ranging from 0.42 mm (40 mesh) – 2 (10 mesh) mm by Forest Concepts and used as received. 5 wt.% Ru/C powder and 2 wt.% Ru/alumina pellets were purchased from Sigma Aldrich and Fisher Chemicals, respectively, and used as received. Methanol (certified ACS Reagent Grade, 99.8%), Tetrahydrofuran, Optima™ was purchased from Fisher Chemicals and used as received. Trans-ferulic acid, DMSO-d_6, pyridine-d_5, Folin-ciocalteau's phenol reagent and sodium carbonate solution were purchased from Sigma Aldrich. Tryptone soy broth (TSB) was purchased from BD (Sparks, MD). Gallic acid was purchased from Acros (New Jersey, USA). Deionized water (Millipore model Direct Q3 UV R) was used for all preparations requiring water.

Feedstock structural characterization. X-ray diffraction (XRD) patterns of pre and post reacted biomass samples were recorded by a diffractometer (Bruker D8) equipped with a CuKα radiation source (λ=0.154 nm) at 40 kV and 40 mA. Scanning electron microscopy (SEM) analysis was performed on an Auriga 60 microscope (Carl Zeiss NTS GmbH, Germany) equipped with a

Schottky Field Emission Gun. All samples were deposited on an adhesive carbon tape and sputtered by a DESK IV sputter unit (Denton Vacuum Inc. NJ, USA) equipped with an Au/Pd target.

Catalyst characterization. XRD patterns of the fresh and spent catalysts were recorded by the same diffractometer. Transmission electron microscopy (TEM) analysis was performed on a Talos F200X transmission electron microscope operated at 200 kV. X-ray energy-dispersive spectroscopy (XEDS) analysis was performed on an Auriga 60 microscope (Carl Zeiss NTS GmbH, Germany) equipped with a Schottky Field Emission Gun (FEG) at an accelerating voltage of 10 kV. A Thermo-Fisher K-alpha + X-ray photoelectron spectrometer equipped with a monochromatic aluminum K-alpha X-ray source (400 μm) was used for XPS. Thermogravimetric analysis (TGA) was performed on catalyst pellets using a TA instruments Q600 SDT thermogravimetric analyzer and differential scanning calorimeter (DSC) using a temperature program of 30 to 700 °C at a heating rate of 10 K min^{-1} under N_2 (30 mL min^{-1}).

Reductive catalytic fractionation (RCF) of herbaceous lignin. 1 g of biomass was added to 20 ml methanol in a 50 ml high-pressure Parr reactor along with 100 mg Ru/C or 250 mg of Ru/alumina catalyst. The reactor was stirred with a magnetic stir bar and heated with a high-temperature heating jacket connected to a variable power supply controlled by a PID temperature controller and a K-type thermocouple to measure the reaction temperature through a thermowell. Once sealed, the reactor was purged three times with N_2 and then pressurized with 40 bars of H_2. The reactor was heated to 250 °C (it takes ~10 – 15 min to reach the set point) and held for 15 h while stirring. Reaction conditions were optimized in our previous studies[5,33,46]. Subsequently, the reactor was cooled in an ice bath until reaching room temperature and the gas phase was released. A portion of the reaction products was filtered for monomer identification and quantification. The

remaining liquid was filtrated through a nylon membrane filter (Whatman®, 0.2 μm) and the filtrate was stored for further analyses. The residual holocellulose was separated using a gooch filter and was dried. Reactions with Ru/C powder were carried out in triplicates.

For the mechanistic studies, reactions were performed at 200 ^{o}C (to slow down the kinetics) using miscanthus as feedstock in hexane (non-polar) and methanol (polar) solvents. For experiments without catalyst, the reactors were filled with 40 bars of N_2. Reactions were run in triplicates

For the catalyst recycling experiments, after the first reaction cycle, the catalyst pellets were removed, washed with methanol, and dried at 60 ^{o}C in an oven. An average of four pellets were used for the recycle experiments and were easily separated from the holocellulose residue using tweezers. The recovered catalyst was weighed and then used for the next recycle experiment (an increase in catalyst mass is observed after each run from adsorbed biomass ash and carbohydrates). Three recycle runs were performed for each feedstock using the recovered Ru/alumina catalyst. Recycle experiments with Ru/alumina pellets were carried out in duplicates.

Lignin monomer identification by GC-MS. The reaction products were analyzed by GC-MS using an Agilent 7890B series GC equipped with a HP5-MS capillary column and an Agilent 5977A series mass spectrometer using Helium as carrier gas. The following conditions were used: injection temperature 250 °C, a column temperature program of 50 °C (1 min), a ramp at 15 °C/min to 300 °C and hold at 300 °C (7 min), and a detection temperature of 290 °C.

Lignin monomer quantification by GC-FID. The reaction products were analyzed with a GC (Agilent 7890B series) equipped with an HP5-column and a flame ionization detector (FID) using Helium as carrier gas. The injection temperature was 300 °C. The column temperature program was: 40 °C (3 min), ramp at a rate of 30 °C/min to 100 °C, then ramp at a rate of 40 °C/min to 300

°C, and hold at 300 °C for 5 min. The detection temperature was 300 °C. The peaks in the GC-FID chromatogram appear in the same order as in a GC-MS chromatogram due to the similarities of the capillary columns. Due to commercially unavailable standards, we quantified the abundance of volatile species using decane as an internal standard and the effective carbon number (ECN) method[31]. The monomer yield (based on the lignin mass content) was calculated based on the integrated areas of the monomer and decane in the GC chromatograms as described in our previous publications[5,46]. The selectivity to aromatic monomers is defined as

$$Monomer\ Selectivity\ (\%) = \frac{Monomer\ yield\ (wt.\%)}{Total\ monomers\ yield\ (wt.\%)} x\ 100$$

Gas composition analysis. The gas component was analyzed using a MicroGC (990, Agilent) with thermal conductivity detector (TCD). The MicroGC is equipped with 4 columns: 1 MS5A column with Ar carrier, 1 MS5A column, 1 PPU column, and 1 PPQ column with He carrier. The setup enables the detection of H_2, He, N_2, CH4, C_2H_6, C_2H_4, C_3H_6, C_3H_8, C_4H_8, CO, CO_2, and O_2 gases.

GPC analysis. Gel permeation chromatography (GPC) analysis was conducted using a Waters 2695 HPLC equipped with a Waters model 2414 refractive index detector (RID) and two Waters Styragel columns (4.6 x 300 mm with packing size of 5 μm) connected in series (Models: HR 3 and HR 4). Tetrahydrofuran (THF) was used as the mobile phase at a flow rate of 0.3 mL/min. The column compartment and the RID temperature were set at 25 °C. After RCF, the filtered reaction solution was evaporated to remove the methanol and the lignin oil was collected for characterization. Lignin-oils were dissolved in THF giving a final concentration of 1 mg/ml. The lignin oil in THF solution was filtered with a 0.2 μm syringe filter prior to GPC analysis. Five polystyrene (PS) standards with peak molecular weights (Mp) of 370-17,600 Da were used for

calibration. The average molecular weight of each sample was calculated based on the retention times of the standards.

Isolation of lignin oligomers. After evaporating methanol from the lignin product solution,10 ml of cyclohexane (to remove monomers from the lignin oil) was added to the viscous lignin oil. The mixture was vortexed for 30 seconds and placed in a sonicating bath for 1 hour. The cyclohexane layer was collected for monomer recovery and fresh cyclohexane was added, vortexed and sonicated for two more monomer removal steps. After the three-time cyclohexane extraction, the residue was mixed with 5 ml dichloromethane (DCM) and vortexed into solution. 5 ml of water was added to remove any water-soluble carbohydrate byproducts. The biphasic water-DCM mixture was vortexed to facilitate mixing, and the DCM phase was separated and evaporated to isolate the lignin oligomer residue for NMR analysis.

Model compound condensation reactions. 50 mg trans ferulic acid was added to 20 ml methanol containing 1 M HCl. The solution was heated at 200 ^{o}C for 2 and 4 hrs.

Nuclear magnetic resonance. Heteronuclear single quantum coherence (HSQC) nuclear magnetic resonance (NMR) spectra of extracted lignin oils and isolated oligomer oils were recorded at 25 °C on an Avance III 400 MHz NMR spectrometer (Bruker). Approximately 30 mg of filtered lignin oil or isolated oligomer oils was dissolved in 500 µl of premixed DMSO-d_6/pyridine-d_5 (4:1) prepared in quartz NMR tubes (NewEra). Data processing was performed using the Mestrelab Research software (mNOVA). Semi-quantitative analysis of the relative abundance of chemical functionalities was performed by integrating the volume of ^{1}H-^{13}C cross peaks and normalizing the integrated volumes by the total integrated volumes of the monolignols as described in Table S2.

XRF analysis. X-ray fluorescence (XRF) of the liquid reaction product from the recycle experiments was performed using a Rigaku wavelength-dispersive X-ray fluorescence (WDXRF) spectrometer.

Machine learning analysis. Principal component analysis (PCA) of different datasets was conducted using the MINITAB software[47,48].

Revival of strains. A loopful of *Staphylococcus aureus* was added to a test tube of 5 ml of tryptone soy broth (TSB) and was incubated at 37 °C for 24 hours. The mixture was further diluted by adding 100 µl of the mixture to another tube containing 5 ml of TSB (used as a 0 h reference for assessing minimum inhibitory content (MIC). This mixture was incubated at 37 °C for 24 hours.

Determination of minimum inhibitory concentration. The minimum concentration required to inhibit microbial growth (MIC) of the lignin oils was estimated by two-fold serial dilution method in 96-well plates following reported methods[49]. Solution concentrations (8, 4, 2 and 1 mg/ml for the lignin oil sample; methanol and bacterial suspension as control) were prepared by two-fold serial dilution with TSB media. 20 µl of the working solution was added to 180 µl of bacterial suspension with $OD_{600\ nm} = 0.05$ (10^6 CFU/ml). With the assistance of a microplate reader and an incubator equipped with a shaker (100 rpm) and a thermostat set to 37 °C, the bacterial growth curves were monitored over a period of 48 hrs with $OD_{600\ nm}$ taken at certain intervals followed by shaking. The minimum concentration that gave no rise in the growth curves was designated as the MIC.

Test of total phenolics content (TPC). The concentration of total phenolic compounds was determined using the methods described by Wu *et al.*[50] The gallic acid standards were dissolved in absolute ethanol and subsequently diluted to different concentrations using DI water. 20 µl of the extracts or standards were mixed with 180 µl distilled water, 100 µl of Folin-ciocalteau reagent

and 0.5 ml 20% sodium carbonate solution. The samples stood at room temperature for 2 hrs. Absorbance of the samples was measured at a wavelength of 765 nm by the Synergy 2 multimode microplate reader (BioTek Instruments, Inc., Winooski, VT). A calibration curve from standards of gallic acid concentrations was used to calculate the gallic acid equivalent (GAE) concentrations of the samples. The results are expressed as milligrams (mg) of gallic acid equivalents per g of lignin oil.

Results and Discussion

Feedstock Characterization

Herbaceous biomass compositional analysis results (from the Idaho National Lab Bioenergy Feedstock Library[26]) are presented in Table 1. On a dry weight basis, these feedstocks contain ~15 – 25 wt. % lignin. Other structural components include cellulose and hemicellulose. Herbaceous lignin contains S, G, and H monolignol in roughly similar fractions across the feedstocks. The S content ranges from 40 to 55 wt.% and falls between that for hardwood (60 – 80 wt. %) and softwood (5 – 20 wt. %)[20].

Table 1. Composition of herbaceous biomass and lignin.

Biomass	%Ash	%Lignin	%Holocellulose	%S	%G	%H	%Ferulate	%Coumarate
Corn Stover	3.5	16.5	66.8	46.3	51.2	2.5	14.0	86.0
Switchgrass	2.0	16.2	62.6	40.2	56.8	3.1	27.0	73.0
Miscanthus	0.5	20.4	70.8	42.8	54.8	2.4	18.0	82.0
Sugarcane Bagasse	7.0	25.6	63.5	53.2	44.8	2.1	34.0	66.0
Wheat Straw	5.5	16.3	55.6	48.4	48.1	3.5	84.0	16.0

Ash, lignin, and holocellulose are reported on weight basis. S, G, H are reported on a relative molar abundance of the monolignols. Ferulate and coumarate percent is reported on a relative molar abundance of the hydroxycinnamates. Holocellulose = cellulose + hemicellulose. Full physico-chemical characterization data is in Table S1a-b.

In addition to the S, G, and H monolignols present in woody biomass, these feedstocks have ferulates and coumarates, unique to herbaceous biomass. They also have a high ash content and the implications of ash on lignin depolymerization will be discussed in a later section.

Mechanistic studies of herbaceous lignin depolymerization

To understand the depolymerization of herbaceous lignin into monomers, we performed mechanistic studies using miscanthus feedstock in non-polar (hexane) and polar (methanol) solvents. These experiments were performed at 200 °C to enable better resolution of reaction transients (Figure 2). Transient data is shown in Figures S2 - S3. Without any hydrogenation catalyst and hydrogen gas, miscanthus depolymerization in hexane gave <1 wt.% monomer yields but >25 wt.% in methanol.

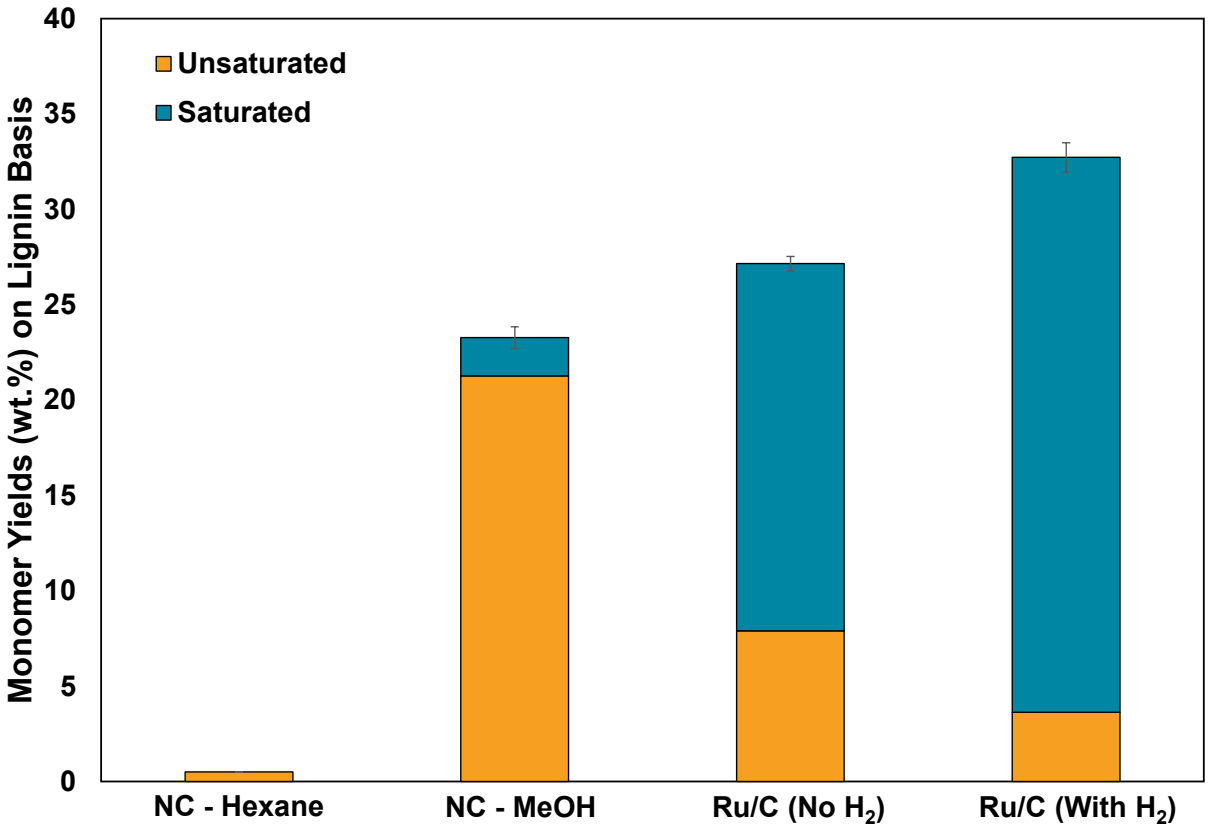

Figure 2. Monomer yield and distribution from miscanthus (MC) depolymerization. NC – no catalyst. Reactions with no catalyst – 1g of miscanthus, 20 ml solvent, 200 ^{o}C, 40 bar N_2. Reactions with catalyst – 1g of miscanthus, 20 ml methanol, 200 ^{o}C, 0.1g Ru/C, 40 bar H_2. Reactions were run for 5 hrs. Error bars are from triplicate experiments.

Results in Figure 2 suggest that a polar solvent[51–53] solubilizes the lignin polymer from the lignocellulose matrix, and fragments[54,55] the polymer into unsaturated monomers. The formation of unsaturated (on the alkyl chain) monomers with no catalyst indicates that lignin β–O–4 cleavage can be facilitated by solvent, shedding more light on existing lignin depolymerization studies[17,20,56,57]. Over Ru/C in methanol, the depolymerization selectively produces saturated lignin monomers (Figure 2 and S1-S2), in contrast to the case with no catalyst (Figure S3 and S4). In reactions without *ex-situ* H_2, H_2 can be generated from the solvent (*e.g.*, methanol, isopropanol, formic acid) by reforming[29,56,58,59], or from formic acid liberated from the hemicellulose fraction during biomass depolymerization[21,60]. Analysis of the gas phase (Table S4) without any *ex-situ* H_2 added confirms the presence of H_2 gas, released *in-situ*, in addition to order gaseous products (CO, CO_2, CH_4, and O_2). Putting these findings together, a hydrogenation catalyst is needed to hydrogenate/passivate the reactive unsaturated monomers, preventing unwanted condensation reactions (Figure 3) and producing a higher yield of monomers (Figure 2).

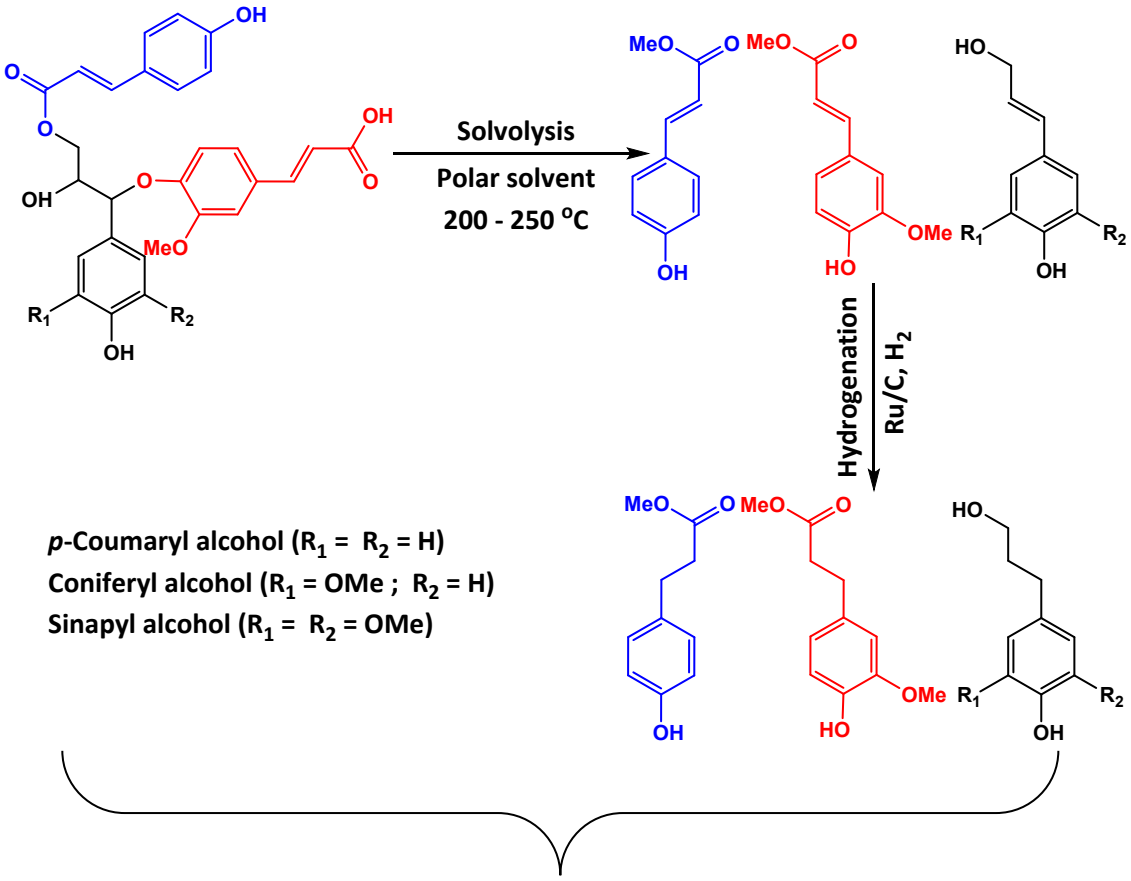

Figure 3. Proposed reaction scheme for herbaceous lignin depolymerization into monomers.

Lignin is first solvolytically extracted and fragmented in a polar solvent at elevated temperatures to yield unsaturated monomers. These monomers undergo passivation over a hydrogenation catalyst (e.g., Ru/C) by H_2, producing saturated aromatic monomers, such as alkyl-guaiacols, syringols, phenols, methyl ferulates, and coumarates. Aside from Ru, other metals, such as Pd and Ni, have been used for lignin RCF. In general, they give similar activities/product yields[38,57,61]. A main difference is that Pd and Ni are selective to lignin monomers with propanol side chain, while Ru is more selective to alkyl sidechain products (due to Ru dehydroxylating the propanol side chain to give propyl side chains). This mechanism applies to both herbaceous and woody biomass (poplar wood was tested giving similar results to miscanthus - Figure S2).

Reductive catalytic fractionation (RCF) of herbaceous feedstocks

With this understanding, we proceeded to perform RCF of the five herbaceous feedstocks. The RCF product yield for each feedstock is shown in Table 2. Phenolic monomers were obtained in good yields and high selectivity to alkyl phenols, leaving behind a high-quality pulp residue. These results indicate the feasibility of obtaining phenolic monomers but with yields widely varying among feedstocks despite having similar β-O-4 content (>90%)[26].

Table 2. Yields (wt. %) and selectivities (%) to products from RCF of herbaceous feedstocks.

		Monolignols			Hydroxycinnamates	
	Monomer Yield* (wt.%)	S_G	S_S	S_H	S_F	S_C
Corn Stover	45.8 ± 1.2	25.0 ± 0.9	30.0 ± 1.2	10.0 ± 1.0	17.0 ± 0.6	15.0 ± 0.7
Switchgrass	41.5 ± 0.9	30.0 ± 0.4	25.0 ± 1.3	9.0 ± 0.9	17.0 ± 0.6	19.0 ± 1.0
Miscanthus	43.8 ± 1.0	40.0 ± 1.0	31.0 ± 0.6	7.0 ± 1.2	11.0 ± 1.2	12.0 ± 0.5
Sugarcane Bagasse	33.7 ± 2.4	22.0 ± 0.2	35.0 ± 0.9	12.0 ± 0.4	8.0 ± 0.8	23.0 ± 1.3
Wheat Straw	20.0 ± 2.2	28.0 ± 0.7	30.0 ± 0.8	12.0 ± 1.2	16.0 ± 0.9	14.0 ± 0.6

*on lignin basis; S - are selectivities to guaiacol (G), syringol (S), ferulate (F), coumarate (C), and hydroxyphenol (H) products. Guaiacol and syringol products include methyl, ethyl, propyl, and propanol substituted products. Reaction conditions: 1 g feedstock, 0.1 g Ru/C, 20 ml methanol, 40 bar H_2, 250 ^oC, 15 hrs.

With 90 % β-O-4 content of these feedstocks, the theoretical monomer yields should be ~ 80 wt.%[21,22,30]. The equation relating the monomer yield to the β-O4 content[21,22,30] is shown below.

$$\text{Monomers yield (mol\%)} \approx (\beta\text{-O4 content})^2$$

However, the monomer yields from 20 – 46 wt.% are much lower than the theoretical ones. All feedstocks had moisture content < 2%, hence the effect of biomass moisture on the catalytic performance was negligible.

Correlating monomer yields across feedstocks *via* simple machine learning

The high abundance of β-O-4[21,22] linkages or of the syringol content[20] in native lignin of woody biomass has been found to correlate strongly with the high aromatic monomer yields in RCF. RCF achieves near-theoretical lignin monomer yields from ether bond cleavage in woody biomass. However, the presence of hydroxycinnamic linkages in herbaceous feedstock complexifies the lignin structure and affects product distribution. To correlate the properties of the feedstock to the RCF depolymerization yields, we employed principal component analysis (PCA) of this modestly high dimensional data (Tables 1 and 2). Two principal components account for 82 % (Figure S5) of the variation in the dataset (Figure 4).

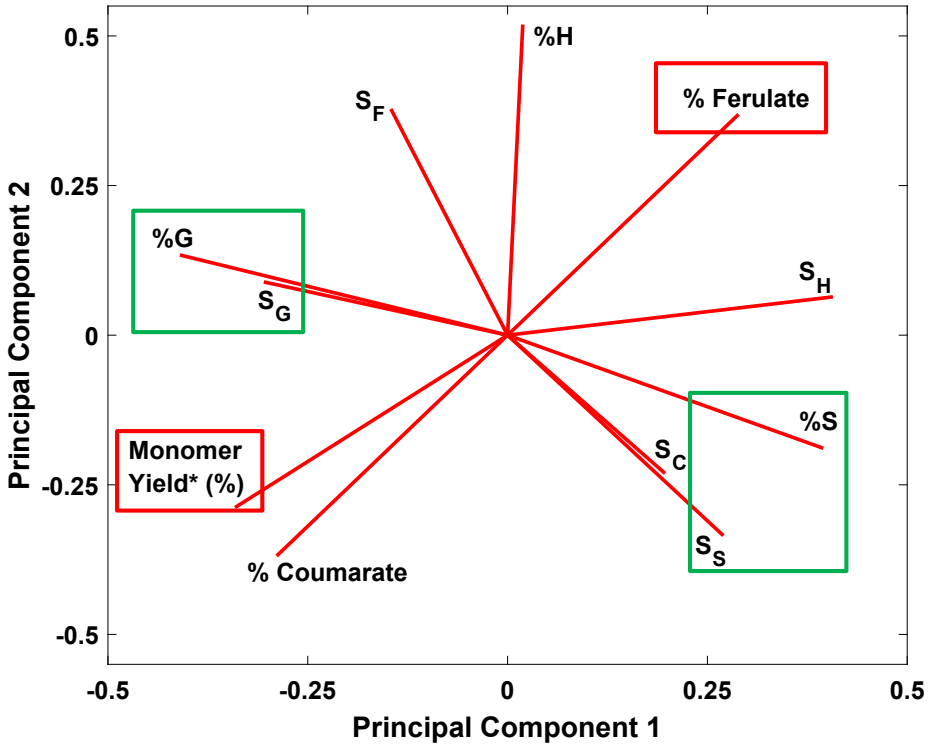

Figure 4. PCA loading plot relating herbaceous lignin monomer yields with lignin composition. S refers to selectivities to guaiacol (S_G), syringol (S_S), coumarate (S_C), ferulate (S_F), and hydroxycinnamic (S_H). S%, G%, and H% refer to the percent of each unit in the lignin. Also included are the total monomer yield, the p-coumarate percent, and the ferulate percent.

Eleven factors, namely the lignin content (syringol, guaiacol, hydroxyphenol, coumarate, and ferulate), the monomer selectivities, and the total monomer yields, are shown in the PCA loadings (Figure 4). Factors that cluster adjacently are positively correlated, those clustered on opposite sides are negatively correlated and those aligned orthogonally are uncorrelated. Clear correlations exist between the lignin composition, the monomer yield, and the product selectivity. Specifically, highlighted in green boxes are positive correlations between the guaiacol (G) content in lignin and the selectivity to G products, the syringol (S) content and the selectivity to S products.

The lack of correlation between the H content and the selectivity to H monomers is due to the decarboxylation[16,17,53,62] of coumarates to form hydroxyphenols. This is evidenced by the H product yields being almost 5 times higher than the H content in the raw herbaceous biomass and the lack of correlation between the C content and selectivity to C products, due to decarboxylation. Interestingly, the ferulate content and the selectivity to ferulate products are also uncorrelated. This indicates an "anomaly" compared to the other lignin components. Furthermore, a strong, negative correlation between the ferulate content and the lignin monomer yield exists (highlighted in red boxes). This suggests that ferulate might limit the monomer yield in herbaceous biomass depolymerization.

Our results suggest that the RCF monomer yields from herbaceous biomass depend on the ferulate content of the feedstocks. This finding is contrary to woody biomass, where the S content correlates with the monomer yields. Shuai *et al*. had postulated the tendency for condensation reactions to occur in herbaceous biomass depolymerization due to the large portion of ferulic acid units[63]. The effect of ferulates on monomer yields is attributed to the possibility of C–C coupling at the α-hydroxyl after cleaving ferulate linkages.

Effect of ferulates on lowering the monomer yields

NMR analysis of the isolated oligomer oils confirmed the presence of non-native α-6 bonds in the oligomer oils (Figure 5). The assignment of the $^{13}C-^{1}H$ correlation peaks in the 2D HSQC spectra for the α-6 bond is 3.62 ppm (δ_{1_H}) and 51.66 ppm (δ_{13_C}) from the NMR database by Ralph *et al*.[64] The H, G and S units of the isolated oligomer oils are shown in Figure S6. These α-6 bonds, absent in the original feedstock are the predominant bonds in the oligomer oils, accounting for 80 - 95 % of the bonds (Table S2). These bonds form as a result of coupling reactions[31] between a benzylic carbocation (after protonation of α-hydroxyl) with an electron rich 6-position on the

aromatic ring of lignin to form an α-6[64] C-C bond (Figure S7). Table S3 shows that feedstocks with high ferulate content have low monomer yields. These high ferulate feedstocks also produce lignin oils with high average molecular weight and high relative α-6 bond content. This, along with the PCA results above, point to the ferulates as the component responsible for lower monomer yields by driving condensation reactions between aromatic monomers to form α-6 linked C-C oligomers.

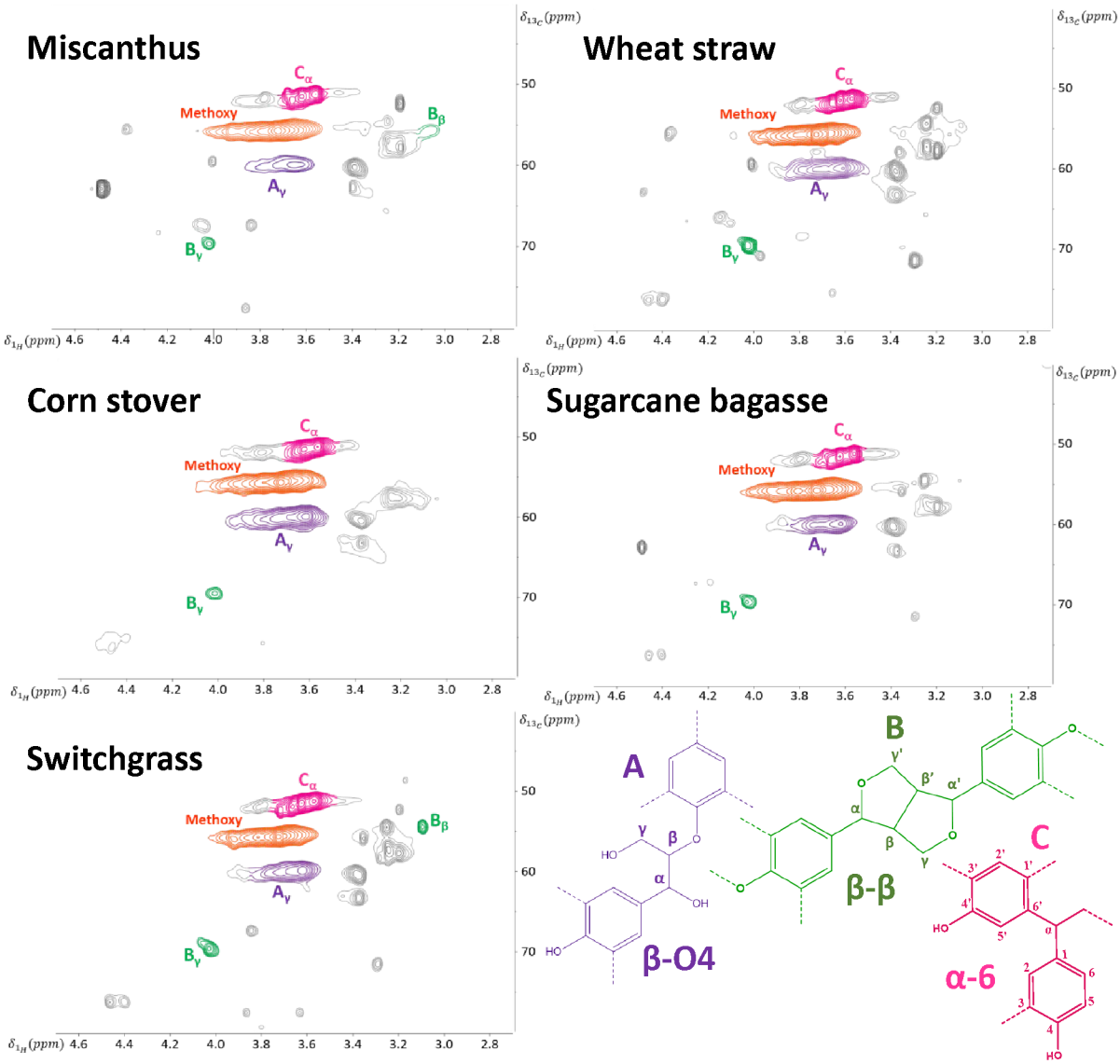

Figure 5. 2D HSQC NMR of the isolated oligomer lignin oils (side chain region). The three bond types identified in the oligomer oils are color coded (purple – β-O4, green – β-β, pink – α-6) to facilitate comprehension of the NMR plots.

To provide experimental evidence of the acid mediated condensation of ferulates, we heated trans-ferulic acid (molecular weight -194 g/mol) in methanol (with and without acid) at 200 ^{o}C. In the absence of acid, only low molecular weight thermal decomposition products (ethyl and vinyl guaiacol) were found. When hydrochloric acid was added, high molecular weight components in the GCMS spectra (300, 326 and 358 m/z) were identified (Figure S8), corroborating our hypothesis on the acid mediated condensation of monomer to oligomers. Our findings support Sturgeon *et al.*'s computational modelling showing that lignin monomer condensation proceeds spontaneously following the formation of benzylic carbocation intermediate[65] following α-hydroxyl group[30,31,63] protonation. This group, abundant in lignin carbohydrate complexes[1,15,66], is easily protonated[31,33,46,63] by acidic components (acetic acid) liberated from the lignin carbohydrate complex[21,37,67] in herbaceous feedstock. This implies that the condensation of reactive carbocations proceeds faster than their reductive stabilization, resulting in less than theoretical monomer yields even in the presence of a hydrogenation catalyst and external H_2.

To minimize the formation of benzylic cations and prevent condensation reactions, Luterbacher *et al*[31,68] showed that aldehydes can form a protective dioxane structure with α- and γ-hydroxyl groups. We performed RCF of miscanthus by adding 1 ml of aldehyde (propionaldehyde and formaldehyde) to the depolymerization mixture to minimize condensation reactions. We observed an increased monomer yield for miscanthus from 43.8 wt.% to 52.0 wt.%

(propionaldehyde) and 50.0 wt.% (formaldehyde). In particular, formaldehyde blocked the reactive electron-rich 2 position to form hydroxymethyl substituted guaiacol and hydroxycinnamic acid products as an alternative anti-coupling mechanism (Figure S9), reducing the formation of C–C condensation linkages. Using reagents, such as aldehydes, that can rapidly block the α-hydroxyls[31,63] to minimize lignin condensation as well as controlled reduction of ferulic acid linkages through genetic engineering[69,70] could be viable approaches to increase monomer yields towards theoretical values.

Effect of herbaceous ash on catalyst recyclability

To investigate the effect of herbaceous biomass ash on catalyst recyclability, we performed RCF experiments using Ru/alumina pellets. Pellets allow facile recuperation of the catalyst from the biomass for reuse and characterization as well as recovery of catalyst-free carbohydrate pulp. Mass balances for all the feedstocks are shown in Table S5. The monomer yields and selectivities for the recycle experiments are shown in Table 3. Lower monomer yields on Ru/Alumina in comparison to Ru/C could be related to differences in Ru dispersion or the H_2 adsorption or the acidity of the support. The interaction of the solvent with the support may also affect the available coverage for the reactive intermediates and H_2 for subsequent hydrogenation. Deng *et al*. had shown, using H_2 temperature-programmed desorption (H_2-TPD), that Ru/C adsorbs H_2 significantly stronger[71] than Ru on alumina and other catalyst supports, providing an explanation for its higher hydrogenation activity[20,38,56,61]. The Ru nanoparticles act as anchoring sites for intermediate lignin oligomeric fragments[72] as well as H_2 atoms[73–75].

Table 3. Monomer yields and selectivity from catalyst (Ru/alumina) recyclability studies.

		Monomer yield (wt.%)	S_G	S_S	S_H	S_C	S_F
Corn Stover	Recycle 1	30.1 ± 0.9	23 ± 1.5	26 ± 1.6	18 ± 1.2	16 ± 0.8	12 ± 1.3
	Recycle 2	28.5 ± 1.1	26 ± 0.6	28 ± 1.0	15 ± 1.1	14 ± 1.0	15 ± 0.5
	Recycle 3	26.6 ± 2.0	23 ± 1.3	35 ± 0.5	14 ± 0.8	12 ± 1.3	13 ± 1.0
Switchgrass	Recycle 1	25.4 ± 1.4	30 ± 0.4	24 ± 1.2	13 ± 0.6	18 ± 0.6	13 ± 1.0
	Recycle 2	24.1 ± 0.8	34 ± 1.0	25 ± 0.6	13 ± 1.2	15 ± 0.4	12 ± 0.8
	Recycle 3	23.8 ± 1.6	32 ± 1.3	24 ± 1.0	13 ±1.0	16 ± 1.2	13 ± 0.8
Miscanthus	Recycle 1	30.4 ± 0.4	32 ± 0.8	26 ± 1.4	11 ± 0.6	11 ± 0.8	13 ± 1.2
	Recycle 2	28.6 ± 1.6	29 ± 0.4	30 ± 1.4	9 ± 0.5	12 ± 1.0	15 ± 0.4
	Recycle 3	28.4 ± 1.2	28 ± 0.5	27 ± 0.8	9 ± 1.0	15 ± 1.2	16 ± 0.8
Sugarcane Bagasse	Recycle 1	23.2 ± 0.9	19 ± 0.9	29 ± 1.1	20 ±0.7	21 ± 1.6	9 ± 0.6
	Recycle 2	21.9 ± 1.5	20 ± 1.8	30 ± 1.2	19 ± 1.4	21 ± 1.8	9 ± 0.9
	Recycle 3	16.6 ± 1.2	17 ± 0.9	27 ± 0.8	20 ± 1.0	24 ± 1.3	8 ± 1.2
Wheat straw	Recycle 1	17.9 ± 0.7	25 ± 1.2	38 ± 0.6	5 ± 0.3	12 ± 1.1	16 ± 1.0
	Recycle 2	16 ± 1.2	30 ± 2.2	31 ± 1.4	6 ± 0.3	14 ± 1.3	15 ± 1.2
	Recycle 3	15.6 ± 1.0	29 ± 0.8	33 ± 1.0	6 ± 0.6	15 ± 1.7	11 ± 0.8

While the product selectivity remains consistent across three runs, the monomer yields decrease with catalyst reuse. This decrease is more pronounced for high ash-content feedstocks (sugarcane bagasse and wheat straw). XRD (Figure 6), XPS (Figure 7), XEDS, and TEM (Figure 8) were performed on the fresh and spent (recovered catalyst after three recycle runs) Ru/alumina catalysts.

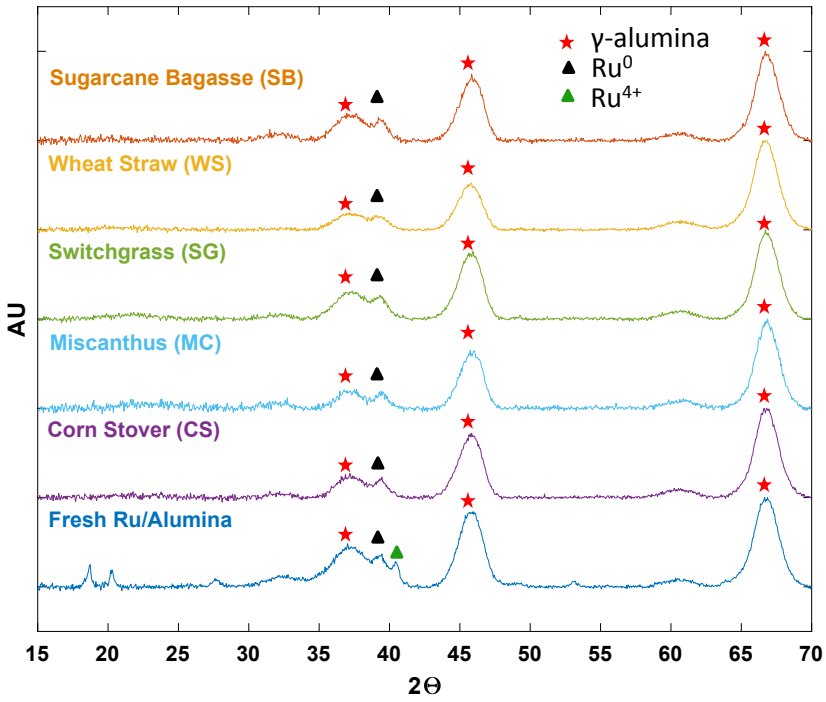

Figure 6. X-ray diffractograms of the fresh and spent catalysts.

Peaks at 37.03°, 46.2° and 67.04° correspond to the γ-alumina support. Peaks at 38.4° and 40.3° are assigned to metallic Ru^0 (JCPDS-06-0663) and RuO_2 (JCPDS-43-1027), respectively. Characteristic peaks of Ru were minimal and not distinct probably due to high metal dispersion (Figure 9a, Figure S10a)[76]. The Ru^{4+} peak is absent in the spent catalysts, indicating reduction to metallic ruthenium during lignin hydrogenolysis.

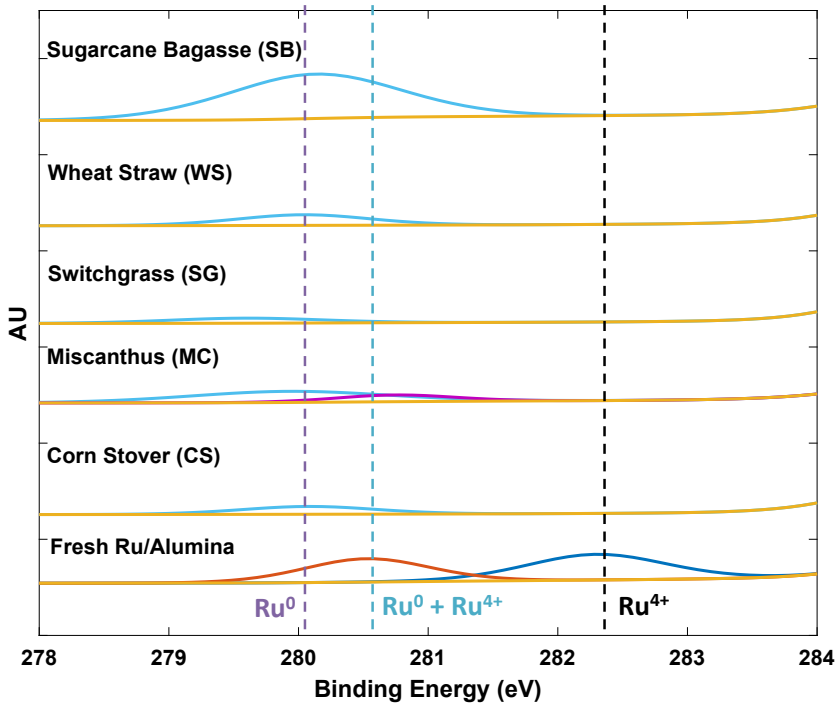

Figure 7. Fitted Ru $3d_{5/2}$ XPS spectrum of the fresh and spent catalysts.

The Ru $3d_{5/2}$ XPS spectrum of the fresh catalyst (Figure 7) shows a peak at 280.6 eV indicating coexistence of Ru^0 and Ru^{4+} and a peak at 282.4 eV indicating Ru^{4+} (RuO_2) consistent with XRD data. For the spent catalyst, there is a shift to lower binding energies (280.1 eV) indicating metallic Ru^0. The signal for metallic Ru is particularly pronounced for the spent catalyst used for sugarcane bagasse. Sugarcane bagasse has the highest amount of ash (Table S1b) amongst the feedstocks used herein, and the high inorganic metal content might induce agglomeration[32,35] of metallic Ru and reduced activity[32]. TEM images (Figure 8) of the fresh and spent catalysts (recovered from sugarcane bagasse RCF) are consistent with catalyst sintering (average particle size of 5.1 nm after the third cycle vs. 2.9 nm of the fresh catalyst). This is further corroborated from XEDS elemental mapping showing highly dispersed Ru nanoparticles in the fresh catalyst but agglomeration of particles in the spent catalyst (Figure S10). This could explain similar yield loss observed for other feedstocks of high ash content (wheat straw and corn stover).

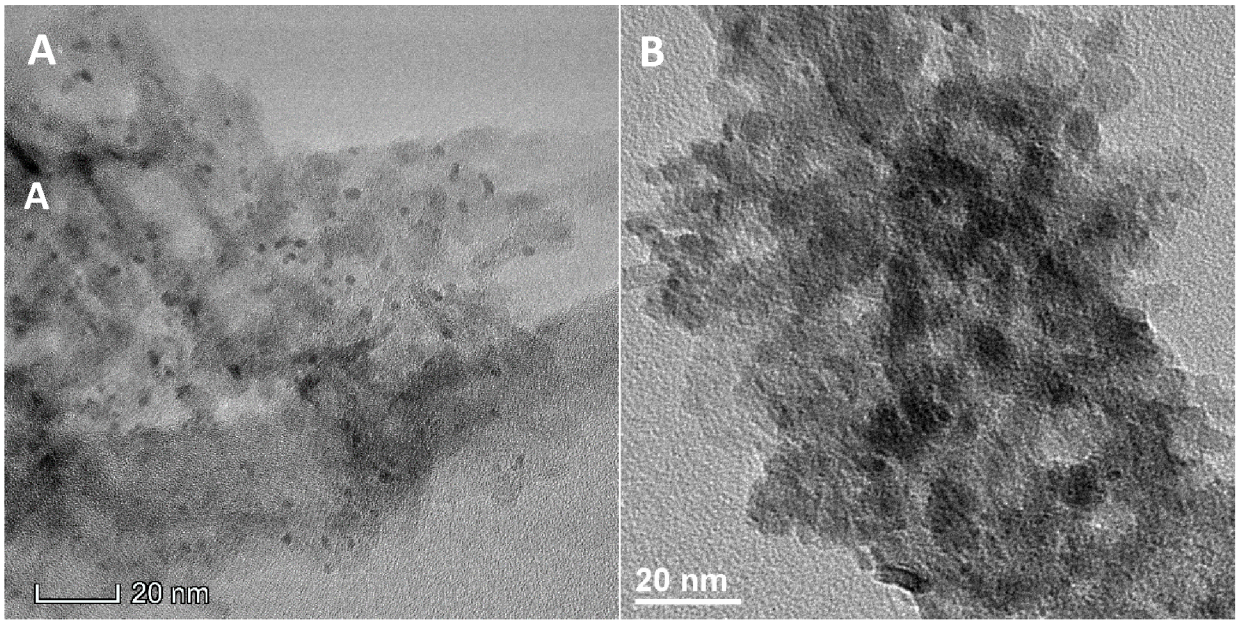

Fig 8. TEM images of A) fresh Ru/Al_2O_3 and B) spent Ru/Al_2O_3 (sugarcane bagasse). More than 200 particles were counted for statistics.

Furthermore, XEDS elemental analysis (Figure S11 and S12) indicates a reduction in Ru content upon use, consistent with metal leaching seen during poplar wood RCF[32,35]. XRF analysis of the reaction solution indicates leached Ru metal along with Si, Ca, Na, Cl, and K (Table S6). Si, K, S, and Na (Table S1b) block catalyst active sites[32,77] and lower monomer yields. Thermogravimetric analysis (Figure S13) of the spent catalysts indicates surface bound lignin oligomers and carbohydrates[35,61] that possibly contribute to catalyst fouling. Specifically, an increase in the recovered catalyst mass of up to 10%, stemming from these surface species, is seen (Table S7). Altogether, these results suggest that sintering, leaching, and fouling are possible catalyst deactivation routes.

Characterization of the RCF pulp residue

We analyzed the recovered carbohydrate residue solids using SEM and XRD. SEM (Figure S14) shows numerous small flakes (<50 μm) compared to the raw biomass samples consisting of

a more fibrous, particulate microstructure (Figure S15 and S16). After RCF, feedstocks with higher ash content, such as wheat straw and sugarcane bagasse, lack sharp crystalline peaks at $2\Theta = \sim 22^{O}$ and 26.5^{O} (Figure 9), evident in the unprocessed feedstocks due to silica[78] (JCPDS-46-1045) components in ash. This supports our findings on leaching of inorganics into the solution (Table S6) which could contribute to catalyst deactivation (Figure 8b and S12). While all the residual pulps have cellulose I structure with peaks at 12.30^{o} $(1\bar{1}0)$, 16.29^{o} (110), and 22.48^{o} (200), the $1\bar{1}0$ plane becomes more prominent for sugarcane bagasse and switchgrass compared to the original biomass feedstock. The metastable state of cellulose I allows the interconversion[79–81] of cellulose I_{α} (triclinic crystal structure) and cellulose I_{β} (monoclinic crystal structure) upon heat treatment, and suggests that pulps of sugarcane bagasse and switchgrass have modified crystalline structure compared to that from the unprocessed biomass. The removal of acid neutralizing inorganics in the residual pulp after RCF provides a more amenable, high quality pulp feedstock in comparison to the raw feedstock for further processing through acid[37] or enzymatic hydrolysis[82].

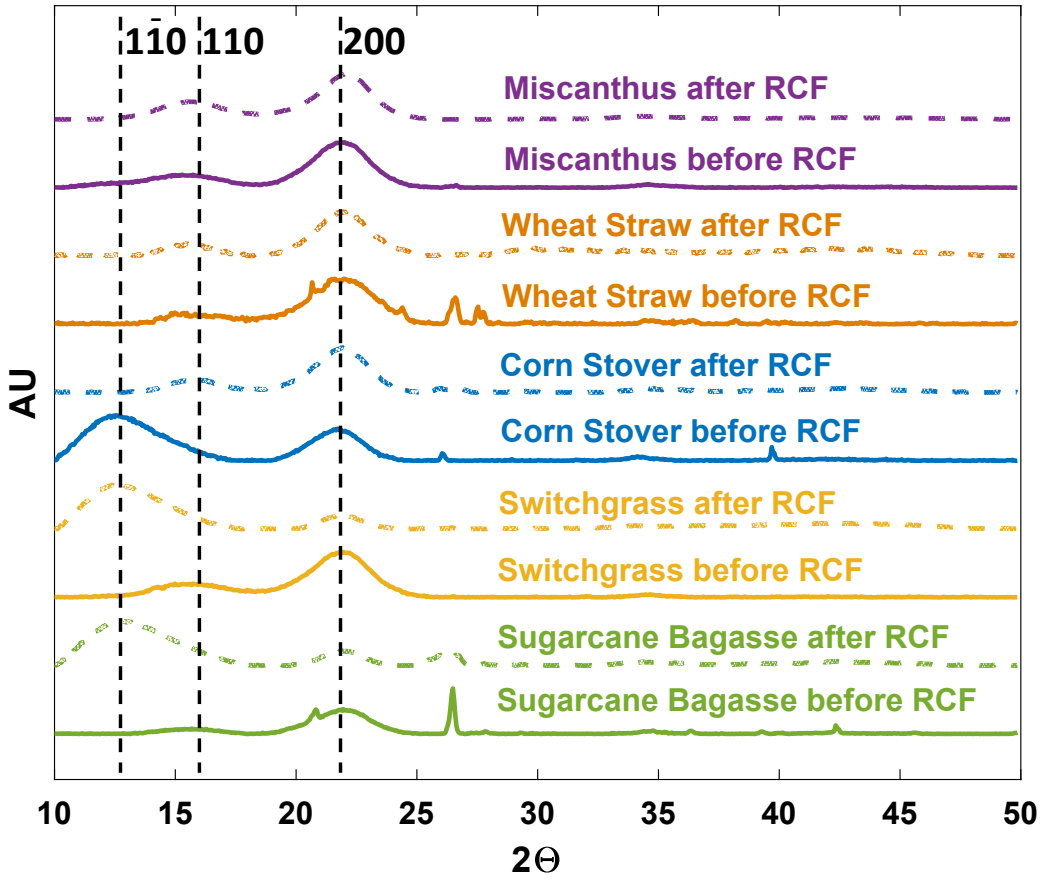

Figure 9. X-ray diffractograms of the herbaceous biomass before and after RCF.

Antimicrobial testing of herbaceous lignin oils

Current annual availability of lignin in herbaceous biomass is estimated to be 100 million tonnes[7]. Based on a ~40 wt.% lignin monomer yield, this translates to an annual production of approximately 40 million tonnes of lignin oil. Recently, lignin monomers have been used for developing polymers[5] and pharmaceutical drug precursors[41]. Here we assess these aromatic compounds as antimicrobial agents. The global antibiotic market size was valued at $7.81 billion[83] in 2017. The application of lignin oil as biobased antimicrobials in food preservatives, pharmaceuticals, disinfectants, and cosmetics could create a new commercial insertion point. However, other factors including extent of oil purity for final applications, compatibility with

product formulations, regulatory requirements, toxicity and final price of these biobased microbials will determine market segments these products can be applied to.

The MIC of the lignin oil from each feedstock on *Staphylococcus Aureus* was determined as a measure of the bacteriostatic activity. In the US, about 500,000 people suffer annually from a staphylococcal infection, mainly by *S. aureus*[84]. MIC is the lowest concentration able to prevent "visible growth" of the microorganism. At this point (usually after 24 hours), if the number of living bacteria (optical density (OD) value of the sample) is lower than that of the control group (bacteria inoculum), the sample possesses antibacterial activity (Figure S17). The MIC for each lignin oil is shown in Table 4. At low lignin oil concentrations, lignin oil from each feedstock inhibits microbial growth. Samples with higher total soluble phenolics possess stronger antimicrobial properties. Hydroxyl (OH) groups could provide delocalized electrons as proton exchangers that could destabilize the cytoplasmic membrane of the microorganisms, thereby reducing the pH gradient across the cytoplasmic membrane, leading to cell death[85]. Carboxylic acid (COOH) groups could also contribute to the antimicrobial[85–88] properties of the lignin oil. Sugarcane bagasse, miscanthus and switchgrass show equally high MIC despite containing different total phenolic content (TPC). This finding indicates that different kinds of phenolic compounds in the three lignin oils (Table 1 and 2) might contribute to the same antimicrobial activities. Switchgrass has the lowest TPC among the three lignin oils (sugarcane bagasse and miscanthus), indicating that its phenolics possess stronger antimicrobial activities. On the other hand, wheat straw with the highest TPC has the second most effective MIC (Table 4), implying that its phenolic compounds impart weak antimicrobial activities against *Staphylococcus Aureus.*

Table 4. MIC of the different lignin oil samples against *Staphylococcus Aureus.*

Samples	MIC (wt. %) of lignin oil against *S. aureus*	Total phenolic content (TPC) (mg/g)
Corn Stover	1.00	33.56
Switchgrass	0.25	59.92
Miscanthus	0.25	96.83
Sugarcane Bagasse	0.25	87.99
Wheat Straw	0.50	119.39

The amount of each lignin monomer obtained from hydrogenolysis as well as the MIC were analyzed using PCA, establishing lignin oil structure - antimicrobial activity relations. Two principal components account for 84 % (Figure S18) of the variation in the dataset. The analysis suggests that four components (methyl coumarate, propyl guaiacol, propyl syringol, and ethoxy phenol) have the strongest bacteriostatic influence (lowering the MIC), with methyl coumarate having the strongest negative correlation with the MIC[10] (Figure S19). The presence of long alkyl chains[85] on the syringol and guaiacol monomers coupled with the absence of the methoxy group[85,89] on the hydroxyphenols and methyl coumarate may be responsible for the antimicrobial activity of these lignin monomers. These results suggest that herbaceous biomass is an ideal feedstock, compared to woody biomass, for producing antimicrobial lignin oils due to its coumarate content.

Conclusions

Waste agricultural residues (corn stover, wheat straw, sugarcane bagasse) and energy crops (miscanthus, switchgrass) were depolymerized using reductive catalytic fractionation (RCF).

Guaiacols, syringols, hydroxyphenols, and hydroxycinnamic esters up to 20 – 45 wt. % (based on total lignin), were obtained, leaving behind a high-quality pulp for further upgrade. Interestingly, depolymerization of β-O-4 lignin bonds to monomer fragments can be achieved by solvent alone, without the need of a hydrogenation catalyst or H_2. Contrary to woody biomass, where the monomer yield is correlated with the syringol-content, PCA indicates that the ferulate, the lignin to carbohydrate crosslinker, negatively impacts the monomer yields. These ferulate linkages undergo acid mediated condensation to form α-6 lignin oligomers, explaining the low monomer yields (in comparison to the theoretical yields) of herbaceous biomass. Metallic ash in the feedstocks deactivates the catalyst by catalyst sintering and fouling and can affect the catalyst recyclability. Therefore, exploring catalysts resistant to high ash content or de-ashing of herbaceous biomass are important future research areas. Even at low concentrations, the lignin oil derived from herbaceous biomass inhibits the growth of *Staphylococcus aureus*, highlighting its potential as a biobased antimicrobial in functional food development and food preservative. Overall, herbaceous biomass with low ferulate (such as corn stover, miscanthus or genetically engineered herbaceous feedstocks with zero ferulate) and ash content would be an ideal agricultural waste feedstock in a "lignin first" biorefinery.

Conflict of interests

The authors declare that they have no competing interests.

Acknowledgements

This work was supported as part of the Catalysis Center for Energy Innovation, an Energy Frontier Research Center funded by the U.S. Department of Energy, Office of Science, and Office of Basic Energy Sciences under award number DE-SC0001004. E.E. also acknowledges support from the Delaware Environmental Institute Fellows Program from the University of Delaware. The authors also acknowledge the use of the Advanced Material Characterization Laboratory (AMCL) and the W.M. Keck Microscopy Facility at the University of Delaware. C. Foster from Great Lakes

Bioenergy Research Center, Michigan State University is thanked for characterizing herbaceous biomass monolignol composition. J. Sloppy is thanked for assistance with the TEM of the catalysts. We thank Idaho National laboratory for providing the (fully characterized) herbaceous biomass samples. Forest concepts is also thanked for milling biomass samples.

Data and materials availability

All data needed to evaluate the conclusions in the paper are present in the paper and/or the Supplementary Materials. Additional data related to this paper may be requested from the authors.

References

1 A. U. Buranov and G. Mazza, *Ind. Crops Prod.*, 2008, **28**, 237–259.

2 U.S. fuel ethanol production continues to grow in 2017 - Today in Energy - U.S. Energy Information Administration (EIA), https://www.eia.gov/todayinenergy/detail.php?id=32152, (accessed 24 October 2019).

3 D. M. Alonso, S. H. Hakim, S. Zhou, W. Won, O. Hosseinaei, J. Tao, V. Garcia-Negron, A. H. Motagamwala, M. A. Mellmer, K. Huang, C. J. Houtman, N. Labbé, D. P. Harper, C. T. Maravelias, T. Runge and J. A. Dumesic, *Sci. Adv.*, 2017, **3**, 1–7.

4 C. O. Tuck, E. Pérez, I. T. Horváth, R. A. Sheldon and M. Poliakoff, *Science*, 2012, **337**, 695–699.

5 S. Wang, L. Shuai, B. Saha, D. G. Vlachos and T. H. Epps, *ACS Cent. Sci.*, 2018, **4**, 701–708.

6 R. A. Sheldon, *ACS Sustain. Chem. Eng.*, 2018, **6**, 4464–4480.

7 U.S. Department of Energy, *U.S. Billion-Ton Update: Biomass Supply for a Bioenergy and Bioproducts Industry*, 2011.

8 W. Schutyser, T. Renders, S. Van den Bosch, S.-F. Koelewijn, G. T. Beckham and B. F. Sels, *Chem. Soc. Rev.*, 2018, **47**, 852–908.

9 Z. Sun, B. Fridrich, A. De Santi, S. Elangovan and K. Barta, *Chem. Rev.*, 2018, **118**, 614–678.

10 K. Pei, J. Ou, J. Huang and S. Ou, *J. Sci. Food Agric.*, 2016, **96**, 2952–62.

11 American Chemical Society, Trans-Cinnamic acid.

12 Solvay, Solvay offers the vanillin the food industry wants today | Solvay, https://www.solvay.com/en/article/natural-vanillin-ensures-resource-efficiency, (accessed

28 January 2020).

13 BASF, Making a difference in the natural F&F ingredients market, https://www.basf.com/global/en/products/segments/nutrition_and_care/nutrition_and_health/aroma-ingredients/our_product_range/flavor-and-fragrance-ingredients.html, (accessed 28 January 2020).

14 US9089499B2 - Para-coumaric acid or para-hydroxycinnamic acid derivatives and their use in cosmetic or dermatological compositions - Google Patents, https://patents.google.com/patent/US9089499B2/en, (accessed 7 January 2020).

15 J. Ralph, *Phytochem. Rev.*, 2010, **9**, 65–83.

16 E. M. Anderson, R. Katahira, M. Reed, M. G. Resch, E. M. Karp, G. T. Beckham and Y. Román-Leshkov, *ACS Sustain. Chem. Eng.*, 2016, **4**, 6940–6950.

17 S. Li, W. Li, Q. Zhang, R. Shu, H. Wang, H. Xin and L. Ma, *RSC Adv.*, 2018, **8**, 1361–1370.

18 P. R. Patwardhan, R. C. Brown and B. H. Shanks, *ChemSusChem*, 2011, **4**, 1629–1636.

19 H. Luo, I. M. Klein, Y. Jiang, H. Zhu, B. Liu, H. I. Kenttä and M. M. Abu-Omar, *ACS Sustain. Chem. Eng.*, 2016, **4**, 2316–2322.

20 S. Van Den Bosch, W. Schutyser, R. Vanholme, T. Driessen, S. F. Koelewijn, T. Renders, B. De Meester, W. J. J. Huijgen, W. Dehaen, C. M. Courtin, B. Lagrain, W. Boerjan and B. F. Sels, *Energy Environ. Sci.*, 2015, **8**, 1748–1763.

21 M. V. Galkin, A. T. Smit, E. Subbotina, K. A. Artemenko, J. Bergquist, W. J. J. Huijgen and J. S. M. Samec, *ChemSusChem*, 2016, **9**, 3280–3287.

22 T. Phongpreecha, N. C. Hool, R. J. Stoklosa, A. S. Klett, C. E. Foster, A. Bhalla, D. Holmes, M. C. Thies and D. B. Hodge, *Green Chem.*, 2017, **19**, 5131–5143.

23 A. Lourenço and H. Pereira, in *Lignin - Trends and Applications*, InTech, 2018.

24 J. del R. C, J. Rencoret, G. Marques, A. Gutiérrez, D. Ibarra, J. I. Santos, J.-B. Jesus, L. Zhang and A. T. Martinez, *J. Agric. Food Chem.*, 2008, **56**, 9525–9534.

25 A. Jensen, Y. Cabrera, C. W. Hsieh, J. Nielsen, J. Ralph and C. Felby, *Holzforschung*, 2017, **71**, 461–469.

26 U.S. Department of Energy, Bioenergy Feedstock Library, https://bioenergylibrary.inl.gov/Sample/BiomassInfo.aspx, (accessed 24 September 2019).

27 J. C. Del Río, P. Prinsen, J. Rencoret, L. Nieto, J. Jiménez-Barbero, J. Ralph, Á. T. Martínez and A. Gutiérrez, *J. Agric. Food Chem.*, 2012, **60**, 3619–3634.

28 J. C. del Río, A. G. Lino, J. L. Colodette, C. F. Lima, A. Gutiérrez, Á. T. Martínez, F. Lu, J. Ralph and J. Rencoret, *Biomass and Bioenergy*, 2015, **81**, 322–338.

29 R. Rinaldi, R. Jastrzebski, M. T. Clough, J. Ralph, M. Kennema, P. C. A. Bruijnincx and B. M. Weckhuysen, *Angew. Chemie - Int. Ed.*, 2016, **55**, 8164–8215.

30 M. Talebi Amiri, S. Bertella, Y. M. Questell-Santiago and J. S. Luterbacher, *Chem. Sci.*, 2019, **10**, 8135–8142.

31 L. Shuai, M. T. Amiri, Y. M. Questell-Santiago, F. Héroguel, Y. Li, H. Kim, R. Meilan, C. Chapple, J. Ralph and J. S. Luterbacher, *Science*, 2016, **354**, 329–334.

32 Z. Sun, G. Bottari, A. Afanasenko, M. C. A Stuart, P. J. Deuss, B. Fridrich and K. Barta, *Nat. Catal.*, 2018, **1**, 82–92.

33 Y. Li, L. Shuai, H. Kim, A. H. Motagamwala, J. K. Mobley, F. Yue, Y. Tobimatsu, D. Havkin-Frenkel, F. Chen, R. A. Dixon, J. S. Luterbacher, J. A. Dumesic and J. Ralph, *Sci. Adv.*, 2018, **4**, 1–10.

34 J. M. Pepper and H. Hibbert, *J. Am. Chem. Soc.*, 1948, **70**, 67–71.

35 E. M. Anderson, M. L. Stone, R. Katahira, M. Reed, G. T. Beckham and Y. Román-Leshkov, *Joule*, 2017, **1**, 613–622.

36 M. L. Stone, E. M. Anderson, K. M. Meek, M. Reed, R. Katahira, F. Chen, R. A. Dixon, G. T. Beckham and Y. Román-Leshkov, *ACS Sustain. Chem. Eng.*, 2018, **6**, 11211–11218.

37 S. Sadula, A. Athaley, W. Zheng, M. Ierapetritou and B. Saha, *ChemSusChem*, 2017, **10**, 2566–2572.

38 T. Vangeel, T. Renders, K. Van Aelst, E. Cooreman, S. Van Den Bosch, G. Van Den Bossche, S.-F. Koelewijn, C. M. Courtin and B. F. Sels, *Green Chem.*, 2019, **21**, 5841–5851.

39 R. Chakrabarti, S. A. Tupy and L. D. Schmidt, *Energy and Fuels*, 2011, **25**, 4763–4769.

40 T. Renders, G. Van den Bossche, T. Vangeel, K. Van Aelst and B. Sels, *Curr. Opin. Biotechnol.*, 2019, **56**, 193–201.

41 S. Elangovan, A. Afanasenko, J. Haupenthal, Z. Sun, Y. Liu, A. K. H. Hirsch and K. Barta, *ACS Cent. Sci.*, 2019, **5**, 1707–1716.

42 Herbalox® Rosemary Extract - Kalsec, https://www.kalsec.com/products/herbalox-rosemary-extracts/, (accessed 26 May 2020).

43 Native Extracts, The Relevance of ORAC (Oxygen Radical Absorbance Capacity) Testing, www.nativeextracts.com, (accessed 6 May 2019).

44 National Renewable Energy Laboratory (NREL), Laboratory Analytical Procedures | Bioenergy | NREL, https://www.nrel.gov/bioenergy/laboratory-analytical-procedures.html, (accessed 25 July 2017).

45 A. E. Harman-Ware, C. Foster, R. M. Happs, C. Doeppke, K. Meunier, J. Gehan, F. Yue,

F. Lu and M. F. Davis, *Biotechnol. J.*, 2016, **11**, 1268–1273.

46 L. Shuai, J. Sitison, S. Sadula, J. Ding, M. C. Thies and B. Saha, *ACS Catal.*, 2018, **8**, 6507–6512.

47 Minitab, Example of Principal Components Analysis.

48 J. Lever, M. Krzywinski and N. Altman, *Nat. Methods*, 2017, **14**, 641–642.

49 S. K. Boda, S. Pandit, A. Garai, D. Pal and B. Basu, *RSC Adv.*, 2016, **6**, 39245–39260.

50 Y. Lu and C. Wu, *J. Food Prot.*, 2010, **73**, 2270–2275.

51 K. Barta, A. De Santi, M. V. Galkin, C. W. Lahive and P. J. Deuss, *ChemSusChem*, 2020, cssc.201903526.

52 N. E. Thornburg, M. B. Pecha, D. G. Brandner, M. L. Reed, J. V. Vermaas, W. E. Michener, R. Katahira, T. B. Vinzant, T. D. Foust, B. S. Donohoe, Y. Román-Leshkov, P. N. Ciesielski and G. T. Beckham, *ChemSusChem*, , DOI:10.1002/cssc.202000558.

53 A. Jensen, J. B. Nielsen, A. D. Jensen and C. Felby, *Chapter 4: Thermal and Solvolytic Depolymerization Approaches for Lignin Depolymerization and Upgrading*, 2018.

54 J. Gierer, *Wood Sci. Technol.*, 1985, **19**, 289–312.

55 K. Sarkanen, *Lignins: occurrence, formation, structure and reactions,* Wiley-Interscience, New York, 1971.

56 Q. Song, F. Wang, J. Cai, Y. Wang, J. Zhang, W. Yu and J. Xu, *Energy Environ. Sci.*, 2013, **6**, 994–1007.

57 Y. Li, B. Demir, L. M. Vázquez Ramos, M. Chen, J. A. Dumesic and J. Ralph, *Green Chem.*, 2019, **21**, 3561–3572.

58 X. Liu, H. Li, L.-P. Xiao, R.-C. Sun and G. Song, *Green Chem.*, 2019, **21**, 1498–1504.

59 I. Klein, B. Saha and M. M. Abu-Omar, *Catal. Sci. Technol.*, 2015, **5**, 3242–3245.

60 M. V. Galkin and J. S. M. Samec, *ChemSusChem*, 2014, **7**, 2154–2158.

61 S. Van Den Bosch, T. Renders, S. Kennis, S.-F. Koelewijn, G. Van Den Bossche, T. Vangeel, A. Deneyer, D. Depuydt, C. M. Courtin, J. M. Thevelein, W. Schutyser and B. F. Sels, *Green Chem.*, 2017, **19**, 3313–3326.

62 C. L. Chambon, M. Chen, P. S. Fennell and J. P. Hallett, *Front. Chem.*, 2019, **7**, 246.

63 L. Shuai and B. Saha, *Green Chem.*, 2017, **19**, 3752–3758.

64 S. Ralph, L. Landucci and J. Ralph, *FPL/DFRC NMR Database*, 2009.

65 M. R. Sturgeon, S. Kim, K. Lawrence, R. S. Paton, S. C. Chmely, M. Nimlos, T. D. Foust and G. T. Beckham, *ACS Sustain. Chem. Eng.*, 2014, **2**, 472–485.

66 D. M. de Oliveira, A. Finger-Teixeira, T. Rodrigues Mota, V. H. Salvador, F. C. Moreira-Vilar, H. B. Correa Molinari, R. A. Craig Mitchell, R. Marchiosi, O. Ferrarese-Filho and W. Dantas dos Santos, *Plant Biotechnol. J.*, 2015, **13**, 1224–1232.

67 P. Ferrini, C. A. Rezende and R. Rinaldi, *ChemSusChem*, 2016, **9**, 3171–3180.

68 W. Lan, M. T. Amiri, C. M. Hunston and J. S. Luterbacher, *Angew. Chemie - Int. Ed.*, 2018, **57**, 1356–1360.

69 Y. Mottiar, R. Vanholme, W. Boerjan, J. Ralph and S. D. Mansfield, *Curr. Opin. Biotechnol.*, 2016, 37, 190–200.

70 D. L. Gall, J. Ralph, T. J. Donohue and D. R. Noguera, *Curr. Opin. Biotechnol.*, 2017, **45**, 120–126.

71 W. Deng, X. Tan, W. Fang, Q. Zhang and Y. Wang, *Catal. Letters*, 2009, **133**, 167–174.

72 Y. Li, S. D. Karlen, B. Demir, H. Kim, J. Luterbacher, J. A. Dumesic, S. S. Stahl and J. Ralph, *ChemSusChem*, 2020, **13**, cssc.202000753.

73 G. Li, J. Han, H. Wang, X. Zhu and Q. Ge, *ACS Catal.*, 2015, **5**, 2009–2016.

74 J. Zhang, J. Teo, X. Chen, H. Asakura, T. Tanaka, K. Teramura and N. Yan, *ACS Catal.*, 2014, **4**, 1574–1583.

75 X. Yang, N. Li, X. Lin, X. Pan and Y. Zhou, *J. Agric. Food Chem.*, 2016, **64**, 8379–8387.

76 P. Betancourt, A. Rives, R. Hubaut, C. E. Scott and J. Goldwasser, *Appl. Catal. A Gen.*, 1998, **170**, 307–314.

77 M. Argyle and C. Bartholomew, *Catalysts*, 2015, **5**, 145–269.

78 R. Abd Rashid, R. Shamsudin, M. A. Abdul Hamid and A. Jalar, *J. Asian Ceram. Soc.*, 2014, **2**, 77–81.

79 Vaniespree Govindan, Salmah Husseinsyah, P.L. Teh and Faisal Tanjung, *Adv. Environ. Biol.*, 2013, **8**, 2620–2625.

80 M. Chaplin, Cellulose, http://www1.lsbu.ac.uk/water/cellulose.html, (accessed 20 October 2019).

81 Y. Nishiyama, J. Sugiyama, H. Chanzy and P. Langan, *J. Am. Chem. Soc.*, 2003, **125**, 14300–14306.

82 M. E. Himmel, S.-Y. Ding, D. K. Johnson, W. S. Adney, M. R. Nimlos, J. W. Brady and T. D. Foust, *Science*, 2007, **315**, 804–807.

83 Grand View Research, Global Antibiotic Resistance Market Size | Industry Report, 2018-2025, https://www.grandviewresearch.com/industry-analysis/antibiotic-resistance-market, (accessed 16 November 2019).

84 Bowersox John, Experimental Staph Vaccine Broadly Protective in Animal Studies, https://web.archive.org/web/20070505050641/http://www3.niaid.nih.gov/news/newsreleases/1999/staph.htm, (accessed 16 November 2019).

85 R. Gyawali and S. A. Ibrahim, *Food Control*, 2014, **46**, 412–429.

86 X. Dong, M. Dong, Y. Lu, A. Turley, T. Jin and C. Wu, *Ind. Crops Prod.*, 2011, **34**, 1629–1634.

87 M. J. Alves, I. C. F. R. Ferreira, H. J. C. Froufe, R. M. V. Abreu, A. Martins and M. Pintado, *J. Appl. Microbiol.*, 2013, **115**, 346–357.

88 D. Hoffman-Pennesi and C. Wu, *J. Appl. Poult. Res*, 2010, **19**, 432–443.

89 C. Cueva, M. V. Moreno-Arribas, P. J. Martín-Álvarez, G. Bills, M. F. Vicente, A. Basilio, C. L. Rivas, T. Requena, J. M. Rodríguez and B. Bartolomé, *Res. Microbiol.*, 2010, **161**, 372–382.

TOC graphic

Lignin monomers obtained from herbaceous biomass in polar solvent (no catalyst) are driven by ferulates undergoing acid mediated condensation reactions into oligomers; lignin oils possess bacteriostatic properties.